Geomorphology 272 (2016) 102–114

Contents lists available at ScienceDirect

Geomorphology

journal homepage: www.elsevier.com/locate/geomorph

Biographical sketch of a giant: Deciphering recent debris-flow dynamics from the Ohya landslide body (Japanese Alps)

Fumitoshi Imaizumi [a,*], Daniel Trappmann [b], Norikazu Matsuoka [c], Satoshi Tsuchiya [a], Okihiro Ohsaka [a], Markus Stoffel [b,d,e]

[a] Faculty of Agriculture, Shizuoka University, 836 Ohya, Suruga, Shizuoka 422-8529, Japan
[b] Dendrolab.ch, Institute of Geological Sciences, University of Berne, Baltzerstrasse 1 +3, CH-3012 Berne, Switzerland
[c] Faculty of Life and Environmental Sciences, University of Tsukuba, 1-1-1 Ten-noudai, Tsukuba, Ibaraki 305-8572, Japan
[d] Department for Earth and Environmental Sciences, University of Geneva, 13 rue des Maraîchers, CH-1205 Geneva, Switzerland
[e] Climatic Change and Climate Impacts Group, Institute for Environmental Studies, University of Geneva, 66 Boulevard Carl-Vogt, CH-1205 Geneva, Switzerland

ARTICLE INFO

Article history:
Received 31 July 2015
Received in revised form 13 November 2015
Accepted 15 November 2015
Available online 18 November 2015

Keywords:
Debris flows
Tree-ring reconstruction
LiDAR DEM
Orthophoto interpretation

ABSTRACT

Debris-flow frequency, discharge, and travel distance are highly catchment dependent and typically controlled by topography, hydrological conditions, and sediment supply. As a consequence, detailed and case-specific investigations are needed to decipher debris-flow histories in order to improve hazard mitigation. This study documents past (ca. 10 years) debris-flow occurrences originating from the Ohya landslide, central Japan, by using a large set of methods including field monitoring, repeat airborne LiDAR, orthophoto interpretation, and tree-ring reconstructions. We demonstrate that the different approaches generally agree on the occurrence of debris flows but that mismatches may exist when it comes to the assessment of areas affected by individual events. These differences may even exceed the usual errors in precision inherent to each of the methods used. In the present case, high-resolution orthophoto interpretation tends to underestimate areas affected by debris flows, especially in the vertical direction, in the absence of lateral movement of the channel bed and as a result of shade and areas under trees. On the other hand, we realize that LiDAR data cannot necessarily be used to distinguish local changes in topography from noise. Tree-ring analyses can help to improve the temporal resolution of the analysis, but may have limitations when it comes to the definition of areas affected by an event because of the point-type nature of data. We conclude that the best and most complete results are obtained by combining multiple methods to improve the spatial and temporal resolution of past debris flows and to delimit areas affected by individual events.

1. Introduction

Debris flows are fast-moving mixtures of water, fines, boulders, vegetation, and air. They often occur in confined channels and have been described as being extremely hazardous as a result of their high velocity, large volumes, and destructive power (Lin et al., 2002; Glade, 2005; Cui et al., 2011). Debris flows are typically initiated through the mobilization of unconsolidated sediment, which is stored in channels, or by shallow landslides through the sudden input of large amounts of water during rainstorms. In addition, rapid snowmelt, rain-on-snow events, or the sudden release of water from glaciers or (landslide) dammed lakes have been identified as triggers of debris flows (Iverson, 1997; Wieczorek and Glade, 2005; Worni et al., 2014; Allen et al., in press). More commonly, however, debris flows were described as being triggered by high-intensity, short-duration downpours or low-intensity, long-duration precipitation events (Stoffel et al., 2011, 2014a,b; Schneuwly-Bollschweiler and Stoffel, 2012).

In addition, debris flow characteristics (such as the frequency, magnitude, and travel distance) differ significantly between catchments as a result of differing catchment topography, hydrological conditions, and/or sediment supply (Fannin and Wise, 2001; Jakob et al., 2005). Detailed knowledge of catchment and debris-flow characteristics are therefore of key importance when it comes to improving site-specific process understanding and appropriate hazard mitigation. Field surveys of debris-flow deposits are one of the possible ways to improve the understanding of debris-flow characteristics (Suwa and Okuda, 1983; Whipple and Dunne, 1992; Cornamusini et al., 2002; Keefer et al., 2003) but will not necessarily provide the temporal resolution needed to understand dynamics, volumes, and return periods of debris-flow events.

Field monitoring has been demonstrated to be one of the best ways to know the timing and flow characteristics of debris flows. Detailed field monitoring has been undertaken in many regions including Europe (March et al., 2002; Hürlimann et al., 2003; Berger et al., 2011a; Arattano et al., 2012) and East Asia (Zhang, 1993; Zhang and

* Corresponding author.
E-mail address: imaizumi@cii.shizuoka.ac.jp (F. Imaizumi).

http://dx.doi.org/10.1016/j.geomorph.2015.11.008
0169-555X/

Cheng, 2003; Hu et al., 2011; Suwa et al., 2011), mostly in torrents with high debris-flow activity. The fact that recurrence intervals of debris flows are often >10 years (e.g., Van Steijn, 1996; Imaizumi and Sidle, 2007) limits the choice of suitable torrents.

LiDAR (light detection and ranging) assessments have become increasingly popular in recent years as they provide detailed information on the evolution and changes in topography and thus allow for a documentation of erosion and deposition processes (Staley et al., 2006; Frankel and Dolan, 2007; Berger et al., 2011b; Bremer and Sass, 2012). Airborne LiDAR is effective for the investigation of larger areas (i.e., >1 km^2), whereas topographic changes in small areas can be detected with high spatial resolution by terrestrial laser scanning (TLS) surveys. The spatial accuracy of the DEM obtained by LiDAR generally ranges from several tens of centimeters to several meters in the horizontal and vertical directions (Bremer and Sass, 2012), which is considered to be sufficient to estimate total volumes of transported sediments as well as areas affected by debris flows. One limitation of LiDAR assessments is the duration covered by a data set, as data only exist since the 1990s. Another weakness of airborne LiDAR assessment is their relatively high cost. Intervals of airborne LiDAR assessment in debris-flow systems are therefore generally in the order of several years.

Aerial photograph interpretation is yet another commonly used method to assess debris-flow histories. Periods that can be assessed with aerial images are generally in the order of several decades and thus (much) longer than those covered by LiDAR data (Crosta and Frattini, 2004; Imaizumi and Sidle, 2007; Brardinoni et al., 2009). Precision of aerial photographs has recently been improved through the orthorectification of images with topographic data from airborne LiDAR (Mackey and Roering, 2011). The approach still has its limitations when it comes to the detection of small mass movements, especially in forested and rugged terrains (Brardinoni et al., 2003; Imaizumi et al., 2008). In addition, the interval between pictures is generally >5 years. Image acquisition by an unmanned aerial vehicle (UAV) has recently been shown to yield good results with respect to changes in topography (de Haas et al., 2014), but the spatial accuracy and breadth of surveyed area still need to be improved for its practical use in debris-flow assessments.

In forested environments, geomorphic processes frequently damage trees and leave evidence of past process activity that can be dated with dendrogeomorphic techniques (Alestalo, 1971; Shroder, 1978; Stoffel et al., 2010). These techniques have been repeatedly applied in the past to reconstruct debris flows on forested cones (Hupp, 1984; Bollschweiler et al., 2007; Stoffel et al., 2008). Debris flows may lead to stem wounding and tilting, root erosion, or stem burial. These disturbances lead to various disturbances such as eccentric growth, abrupt changes in growth rates, or local destruction of the cambium and related anatomical reactions after wounding. These growth disturbances can be dated by visual inspection and/or interpretation of the growth-ring series and enable precise dating of past events (Stoffel and Bollschweiler, 2008; Stoffel and Corona, 2014). Dendrogeomorphic techniques require intensive fieldwork and laboratory analysis, but recently established guidelines assist in defining sampling positions on debris-flow cones and therefore help in optimizing sample sizes (Schneuwly-Bollschweiler et al., 2013; Stoffel et al., 2013). Dendrogeomorphic analyses of debris flows have predominantly been realized with conifers, but the potential of broadleaved trees has been recently demonstrated as well (Arbellay et al., 2010, 2014a,b). Using dendrogeomorphic techniques, precise (annual to subannual resolution) and century-long, continuous records of debris flow occurrence can be established. Assessments can also yield data on various debris-flow parameters, such as temporal frequency, estimates of event magnitudes, or analysis of triggering conditions. Furthermore, the dendrogeomorphic dating of landforms created by debris flows enables determination of the spread and reach of past events on forested debris-flow cones (Stoffel et al., 2008; Bollschweiler and Stoffel, 2010).

For a better understanding of debris-flow characteristics and process dynamics at a given site, one needs to select the best and most appropriate methods, taking into account debris-flow frequency, flow characteristics, and available data. Advantages and limitations of each method should be known before an appropriate approach is being defined. In the past, however, most research focused just on the evaluation of errors and the description of limitations of single approaches (Brardinoni et al., 2003; Bremer and Sass, 2012). By contrast, a comparison and/or combination of different methods have not been done in sufficient detail.

The purpose of this paper therefore is to compare characteristics, advantages, and limitations of different assessment methods to study debris flows and to apply them to a specific case where process activity has been very high in the recent past. We investigate the debris-flow history out of the Ohya landslide, central Japan, by using field monitoring, airborne LiDAR DEMs, orthophoto interpretation, and tree-ring assessments. The Ohya landslide, one of the largest landslide bodies in Japan, is appropriate for such a comparison because of the very high debris-flow frequency (with 3–4 events per year; Imaizumi et al., 2005). In addition, various kinds of monitoring and surveys aimed at disaster mitigation have been conducted in this area. This study focused on the most recent debris-flow history (approximately a decade) of the site.

2. Study site

The Ohya landslide, in the southern Japanese Alps (Fig. 1), was initiated during an earthquake in A.D. 1707 and has an estimated total volume of 120 million m^3 (Tsuchiya and Imaizumi, 2010). Unstable material has subsequently been supplied into the channels in the old landslide scar and has affected the occurrence of debris flows ever since the original failure.

The climate at the site is characterized by high annual precipitation (about 3400 mm). Heavy rainfall events (defined here as events with total rainfall >100 mm) occur during the Baiu rainy season (June and July) and the autumn typhoon season (August to October). Most debris flows at the Ohya landslide occur during these seasons, and we refer to this time window (from June to October) as the *debris-flow season*. The main geological units at the site are comprised of highly fractured shale and well-jointed sandstones of Tertiary age. The highest point of the landslide is the north peak (2000 m asl), while the lowest point is at the south end of the landslide at an elevation of 1060 m asl.

Most debris flows occur in the Ichinosawa catchment, which is located at the northern end of the Ohya landslide (Fig. 1B; Imaizumi et al., 2005). This catchment is divided into two sections, the upper and lower Ichinosawa subcatchments. The upper Ichinosawa catchment is a debris-flow initiation zone, whereas the lower Ichinosawa catchment represents the transportation and deposition zones.

Total length of the channel in the upper Ichinosawa catchment is ≈650 m and the south-facing catchment has an area of 0.22 km^2. Anthropogenic influence on debris-flow activity is clearly absent in the area because of the steepness of the site and the harsh environmental conditions. Seventy percent of the basin slope is bare (scree and outcrop), whereas the remaining 30% is vegetation-covered (forest, shrubs, and tussocks). Most of the catchment is characterized by rocky sequences with some high, subvertical walls. The typical gradient of hillslopes is 40–50°. Unconsolidated debris, ranging from sand to boulders, is the main source of debris-flow material (Imaizumi et al., 2006). The thickness of debris deposits attains several meters in some sections. Channel gradients range from 16° to 28° between P1 and P3 (Fig. 1), where channel bed is alternatively composed of deposited sediments and bedrock. Sediment infilling of the channels is dominated by freeze-thaw processes that promote dry ravel, the gravitational transport of surface materials by rolling, sliding, and bouncing across the surface, and rockfall because of the steep hillslopes (Imaizumi et al., 2006).

After the initiation in the upper Ichinosawa catchment, debris flows are transported onto the fan, which is in turn located in the lower Ichinosawa catchment. Length and gradient of the channel in the lower catchment are 600 m and 18°, respectively. Rather young (<20 years) pioneer riparian forests (e.g., *Alnus hirsuta*, *Alnus firma*)

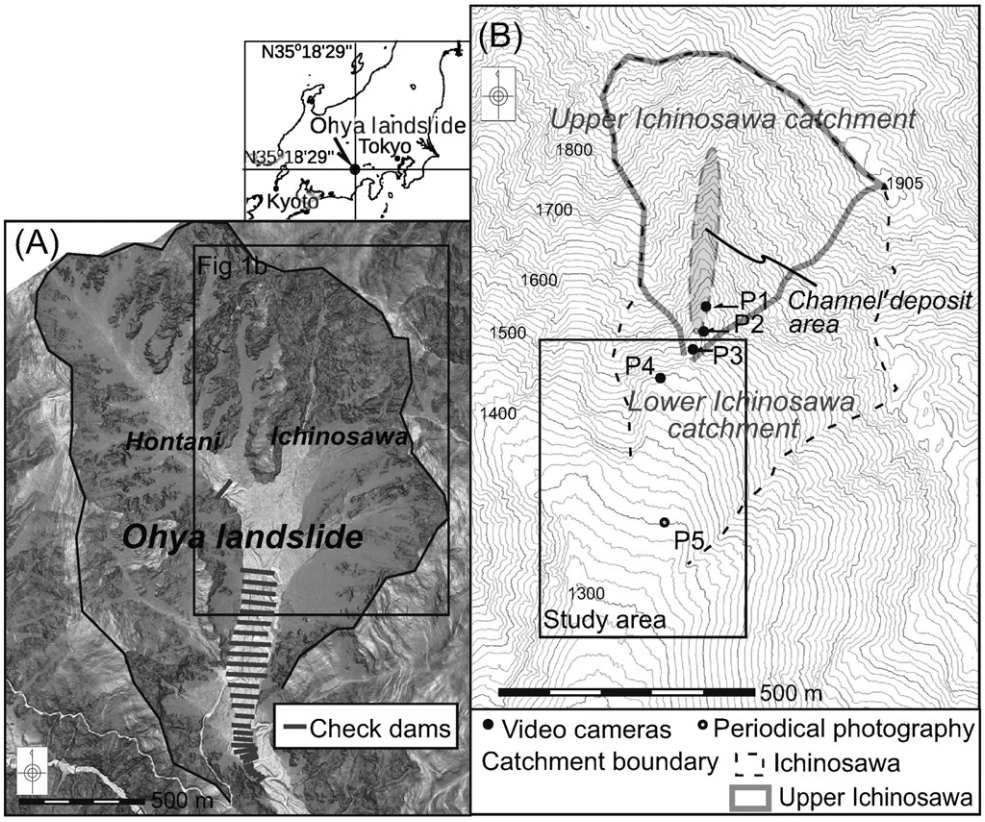

Fig. 1. Map of the Ohya landslide. (A) Landslide body with slope gradients; steeper terrains are expressed as dark colors and gentler terrains are expressed as light colors. (B) Topographic map of Ichinosawa catchment.

partly cover the fan but very frequently are damaged or even removed by debris flows. The Ichinosawa torrent joins the Hontani torrent at the lower end of the lower Ichinosawa catchment at about 1300 m asl (Fig. 1) to become the Ohya River. Surface flow is rare during rainfall events without debris flows because of surface water infiltration into the highly permeable channel deposits. Therefore, changes in topography are above all related to debris-flow events. Noteworthy, a temporary road was constructed in the upper Ichinosawa catchment so as to install monitoring devices in 2009 and 2010.

In addition, 26 check dams with a height of about 5 m, aimed at stabilizing channel deposits, were constructed downstream of the confluence of Ichinosawa torrent with Hontani torrent between 1916 and 1973. All check dams were filled with sediment well before the start of the surveying period. Another large check dam with a height of 14.5 m is located in the Hontani torrent. No debris flows currently occur at the Hontani torrent because of the stabilization of channel deposits by this check dam.

3. Material and methods

3.1. Debris-flow monitoring

The monitoring system at the study site was installed in the upper Ichinosawa catchment in spring 1998 and includes an interval video camera, water pressure sensor, and rain gauge (Imaizumi et al., 2005). The interval video camera provides motion images of in-channel debris flows and allows discrimination of debris-flow occurrences. The video camera was initially installed at P4 in 1998, then moved to P2 in 2000. The interval video camera captured channel images for 0.75 s at an interval of 5 min during the period 1998 to 2001. We shortened this interval to 3 min in April 2001 to capture flow behavior in more detail. In addition, continuous monitoring cameras were installed at P1 in 2003, then at P3 and P2 in 2004 and 2005, respectively. Recording was initiated by wire motion sensors installed at several cross sections in the channel. Since then, one or both video cameras have captured 25 debris flows from locations along P1, P2, and P3. Debris flows cannot be identified on images recorded at night. In addition, we sometimes failed to capture debris flows partly or fully because of mechanical problems with the system affected by harsh site conditions. Therefore, video images are mostly inappropriate for the estimation of total or peak discharge of debris flows. In this study, video images were mainly used to check for the occurrence of debris flows.

Semiconductor type water pressure sensors that monitored hydrostatic pressures up to 49 kPa (accuracy of ±3%) were installed in holes dug in the bedrock of the channel bed and were secured with mortar. To prevent the effect of hydrodynamic pressure changes, the intakes of the sensors were covered by cobbles and mortar. The logging interval was set at 1 min. The water surface height was determined by dividing the measured hydrostatic pressure by the mass density of muddy water, assumed to be 1 g/cm^3. Ultrasonic sensors, with a measuring range from 120 to 600 cm and an accuracy of ±0.4%, were also installed to measure the debris-flow surface height and to draw a debris-flow hydrograph at 1-min intervals. Ultrasonic sensors have lower risks to be broken by debris flows but cannot measure flow height if the flow surface is not flat. Because the duration of one debris-flow surge is generally lasting <1 min (Imaizumi et al., 2005), a high possibility exists that water pressure sensors and ultrasonic sensors will fail to measure the flow height at the peak of a surge. During the passage of debris flows, hydrographs obtained by the instruments show abrupt and intense changes in discharge, whereas such abrupt changes were absent during those rainfall events which did not trigger a debris flow. Therefore, we used flow hydrographs to identify the occurrence of debris flows at the study site. We are well aware that our assumption of the mass density of muddy water (1 g/cm^3, same as clear water) may cause some overestimation of water surface height because the density is generally higher than clear water (sometimes >2 g/cm^3;

Coussot and Meunier, 1996; Hu et al., 2011). The overestimation, however, will not affect debris-flow detection, which was not based on water height (and discharge) value itself but on abrupt changes in discharge.

3.2. Airborne LiDAR scanning

Geodetic surveys were performed seven times between 2005 and 2013 by airborne LiDAR scanning. Six surveys were conducted after the typhoon season (usually from August to October) and before the first snowfall (which typically occurs around mid-December; Table 1). The remaining survey was realized in spring 2009. These seasons are optimal for scanning because leaves of deciduous trees and snow cover are absent. The maximum error in the vertical direction could therefore be limited to about 30–40 cm.

We define the study site for the LiDAR analysis with a width of 400 and a length of 550 m on the debris-flow fan of the lower Ichinosawa catchment (Fig. 1B). To reduce errors related to the positioning of the aircraft, the DEMs from 2006, 2009, 20,010, 2011, 2012, and 2013 were adjusted through comparison with those obtained in 2005. The sum of the square of difference in elevation between the six DEMs and the 2005 DEM in the stable areas (2700 m^2) of the study site was calculated with changing elevation at 0.1 m step. The value giving the smallest square of difference was then used to adjust elevation. As a result of the adjustment, mean and standard deviation of the difference in elevation in stable areas between two consecutive DEMs were smaller than 0.1 and 0.3 m, respectively (Table 2). Changes in ground surface levels resulting from debris flows were then calculated from differences in elevation between pairs of DEMs. Grain size measurement by the line grid method revealed that 95% of the ground surface sediment in the study area was <0.3 m, thereby areas with changes in elevation in excess of 0.3 m were considered to be affected by debris flows.

We then mapped debris-flow lobes (and snouts), which are a typical feature in deposition zones (e.g., Suwa and Okuda, 1983; Whipple and Dunne, 1992) using the LiDAR DEM data. A number of indices, including curvature, roughness, and slope gradient (e.g., Staley et al., 2006; Frankel and Dolan, 2007; Roering et al., 2013) were used to detect debris-flow depositional zones in previous studies. At the Ohya landslide, debris-flow lobes are clearly identified on the maps with gentle slopes on top of lobes surrounded by the steep topography around the front and sides of lobes.

3.3. Estimation of debris-flow volumes

At the Ohya landslide, debris-flow volume (or, more strictly, the total volume of sediment transported by debris flows) can be estimated from changes in the volume of storage (i.e., channel deposits and talus slopes). Debris-flow volume cannot be estimated from LiDAR DEMs as sediment supply from hillslopes and excavation of deposits by debris flows occur in the same interval of LiDAR scanning. Instead, we estimated debris-flow volume from the volume of storage assessed by periodic photography from sites P1 and P5 (Fig. 1). In the upper Ichinosawa catchment, the largest proportion of channel deposits are supplied from the hillslopes that are affected by freeze-thaw processes during winter and early spring (Imaizumi et al., 2006). Evacuation of sediments, by contrast, occurs only during the debris-flow season. Therefore, differences in volume of stored sediment before the start and after the end of a debris-flow season will provide an estimate of the volume of sediment being transported by debris flows. Photographs from site P5 cover the entire upper Ichinosawa catchment, whereas those from P1 show accumulation conditions of channel deposits at the bottom of the deeply incised main channel (which tends to be shaded in photographs taken from P5).

Volume of storage was estimated from the area covered by sediments as assessed by using photographs from P1 and P5 as well as the bedrock topography obtained by airborne LiDAR scanning in the periods when storage was almost absent in the catchment (i.e., in 2011 and 2012). If we assume that LiDAR DEMs provide the true volume of channel deposits, the root mean squared error (RMSE) of the procedure used herein was 5361 m^3. This RMSE is larger than the volume of small debris flows (<2000 m^3) but smaller than the annual volume of sediment supply (>10,000 m^3).

3.4. Orthophoto interpretation

Aerial photographs in the study area were taken together with airborne LiDAR scannings. Orthophotos were constructed from the aerial photographs and DEMs obtained by LiDAR scanning. Seven generations of orthophotos (2005, 2006, 2009, 2010, 2011, 2012, and 2013) were analyzed to quantify geomorphic changes in fan morphology in the lower Ichinosawa catchment between successive scenes. The natural-color digital orthophotos are three-band (red, green, blue) photographs with a resolution of 0.2–0.4 m and a mapping scale of 1:1000. The assessment of positional errors was realized for each generation of orthophotos and through comparison of 13 test points distributed across the stable areas. Test points are mainly anthropogenic features (e.g., roads, check dams) but because of the absence of these features in the upper catchment area also included are center points of stable tree canopies. The distance between corresponding test points (in x and y direction) was considered to represent the locational error (Hughes et al., 2006) that is composed of geopositional errors in the orthophotos and the ability of the interpreter to correctly map features on the screen. The 90th percentile value of test-point errors is 1.2 m in our case (Fig. 2), meaning that positional errors of mapped geomorphic changes are smaller than 1.2 m with a probability of 0.9.

Table 2
Mean and standard deviations of difference in elevation between two consecutive DEMs (adjusted DEMs), which are constructed at the beginning and end of each analysis period in Table 1, in the stable areas.

Period	Debris flow seasons	Mean (m)	Standard deviation
1	2006	−0.008	0.277
2	2007, 2008	0.050	0.221
3	2009, 2010	−0.071	0.164
4	2011	0.040	0.161
5	2012	0.024	0.101
6	2013	−0.072	0.091

Table 1
Measurement period and grid size of DEMs and orthophotographs.

Measurement period		Grid size of DEMs (m)	Resolution of orthophotographs (m/pixel)	Analysis period
Start	End			
December 16, 2005	January 28, 2006	1.0	0.20	1
November 13, 2006	December 5, 2006	1.0	0.40	2
May 9, 2009	May 20, 2009	1.0	0.40	3
November 11, 2010	November 14, 2010	1.0	0.40	4
October 27, 2011	November 3, 2011	1.0	0.25	5
November 7, 2012	December 7, 2012	1.0	0.25	6
November 30, 2013	December 14, 2013	1.0	0.25	

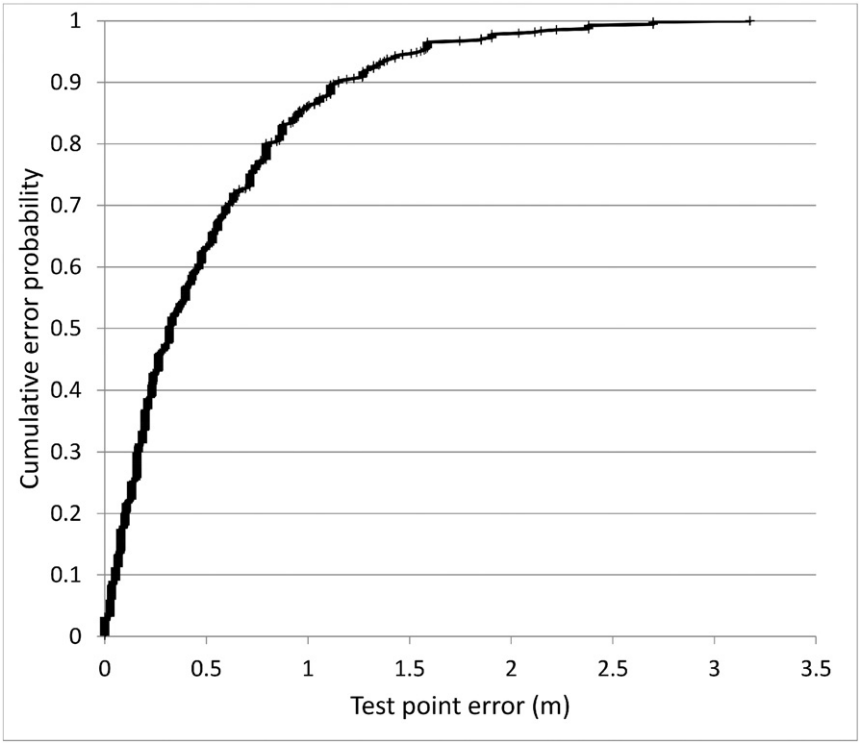

Fig. 2. Cumulative frequency of absolute test-point errors derived from deviations of test points for (all 21) possible combinations of the seven orthophotos analyzed.

Geomorphic change detection focused above all on the visual inspection and mapping of debris-flow-affected areas. After previous field visits on the cone, active flow paths, as well as changes adjacent to the channels (like erosion and deposition zones) were extracted from each scene and synthesized via analytical interpretation. Primarily gray linear features (channels) without vegetation and gray lobe-shaped features were recognized as debris-flow-affected areas and directly delineated on the screen.

3.5. Dendrogeomorphic analysis

A total of 101 samples (wedges and stem disks) were collected from 75 broadleaved trees in October 2014 (Table 3). At the Ohya landslide, mostly young trees are growing that are easily scarred by debris flows because of their thin and fragile bark (Stoffel and Perret, 2006; Trappmann and Stoffel, 2013). Therefore, the high activity enables identification of numerous debris-flow-related landforms that can doubtlessly be dated by tree damage. Analysis thus focused on recent scars visible on disturbed trees along the present-day or recently abandoned flow channels. Samples were sanded with increasingly fine sanding paper (up to 800 grit) before tree rings were counted from bark to pith allowing accurate dating of injuries and thus debris-flow events. The oldest individual reached sampling height at A.D. 1950 (65 years). The mean number of rings present on the samples is 11 years (SD 8 years) but is also affected by the sampling strategy that favored the extraction of wedges where the pith is not normally reached. Mean diameter of sampled trees at breast height accounts to only 7 cm (SD 3.6 cm). The relatively short tree-ring record of mostly juvenile trees did not allow using conventional cross-dating procedures. Therefore, dating confidence was rated qualitatively during the dating process, depending on the quality of the wood samples as well as the visibility of tree rings. Spatial errors are related to the precision of the GARMIN GISMAP 62SCJ such that positioning errors of sampled trees are estimated at <5 m.

Table 3
Tree species sampled for spatiotemporal debris-flow reconstruction.

Species	N	%
Alnus hirsuta	50	67
Alnus firma	6	8
Betula grossa	6	8
Salix sachalinensis	5	7
Acer capillipes	2	3
Fraxinus lanuginosa	2	3
Acer palmatum	1	1
Pterocarya rhoifolia	1	1
Unknown	2	3
Total	75	100

Scars can in general be dated with subannual precision. The seasonality of debris flows was assessed by observing the radial position of the injury within the increment ring (Alestalo, 1971; Stoffel et al., 2005). Following Arbellay et al. (2010), tree rings were subdivided into early earlywood (EE) and late earlywood (LE), followed by a very limited latewood (L) part (Fig. 3). Production of EE starts in late spring. Injuries in this portion of the tree ring were attributed to debris flow events in spring and summer. Production of LE roughly lasts until the end of summer, so events affecting this part were attributed to summer and early autumn. In autumn, L is formed, so events were attributed to early autumn to late autumn. Debris flows occurring outside the growing season cannot be precisely dated but will be evident in the earliest cell layers (dormancy, D; Stoffel et al., 2005; Stoffel and Hitz, 2008) of the growth ring formed in the next growing season. As monitoring data show that events in early spring usually do not occur, events in D were consequently attributed to late autumn of the previous year.

4. Results

4.1. Debris flow events

Fifty debris flows have been monitored for the period 1998–2013 (Fig. 4), resulting in an average annual number of 3.3 events. At least one debris flow occurred each year at the study site: a total of five debris

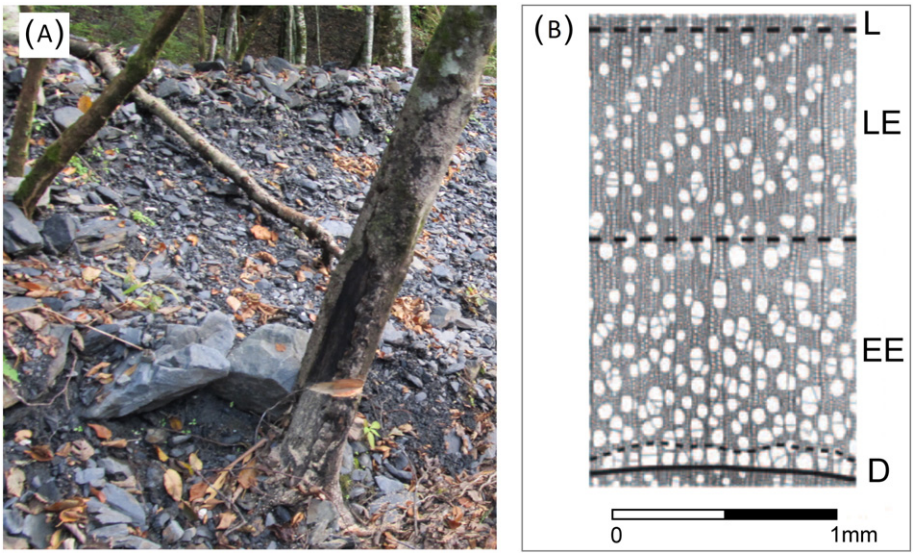

Fig. 3. (A) Wedge-shaped samples were extracted from a large set of trees impacted by debris flows. (B) Annual tree-ring formation can be subdivided into cell layers, which can then be used for the intra-annual dating of events. Injuries during the vegetation period can be attributed based on their position within the tree-ring to early earlywood (EE), late earlywood (LE), or latewood (L) (adapted from Arbellay et al., 2010); injuries outside the vegetation period will leave evidence in the first layers (dormancy, D) of the ring formed in the next vegetation period.

flows occurred in 2000, 2003, 2011, and 2012; whereas only one event was on record in 2002 and 2009. Thirty-six debris flows were not or only partly recorded by the observation system because of malfunction of devices. Nevertheless, the exact occurrence dates of all debris flows, except for one event that occurred sometimes between 10 May and 28 June 2013, could be reconstructed with the help of the monitoring devices and/or changes in topography as detected by field surveys. Also, all debris flows occurred during or soon after intense rainfall events. Twenty-four out of twenty-eight debris flows, for which initiation timing is known with an accuracy of a few minutes, had 10-min rainfall intensities ≥5 mm. The other four debris flows occurred after slightly lower rainfall peaks (3.5 to 5 mm per 10 min). We also realize that the duration of debris flows was typically longer during long-time rainfall events, often related to typhoons in summer and autumn, and sometimes exceeds one day. By contrast, the duration of debris flows caused by short-time rainfalls, such as summer thunderstorms, was much smaller than 30 min. Data also shows that debris flows at the Ohya landslide are usually composed of a sequence of surges. Debris flows triggered by thunderstorms include only few surges, whereas debris flows triggered during long-lasting rainfalls typically had dozens of surges.

Photogrammetric analysis revealed that the total volume of sediment transported from the upper Ichinosawa catchment was highly variable between years (Fig. 4B). Total volume exceeded 50,000 m^3 in 2011 when two massive typhoons with total precipitation >500 mm each affected the region. The total volume of transported sediment in 2009 and 2010 was, by contrast, <5000 m^3. Total volume of transported sediment for each analysis period of the airborne LiDAR survey was also variable (Fig. 4C). In the case of period 4, which includes the 2011 debris-flow season, the highest volumes were recorded; whereas period 3 showed the smallest values despite the fact that this period included two debris-flow seasons (2009 and 2010).

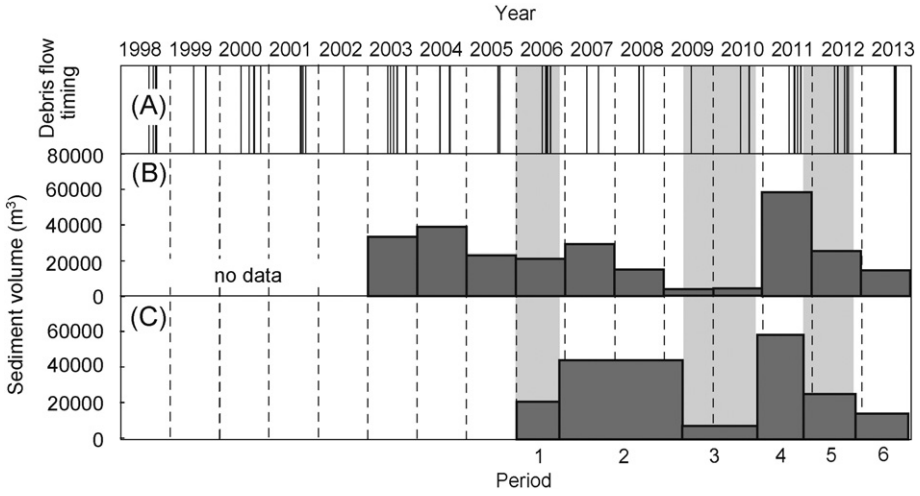

Fig. 4. Timing of debris flows and sediment volumes transported from the debris-flow initiation zone. (A) Timing of debris flow events detected by video cameras, ultrasonic and water pressure sensors, and field surveys. (B) Total annual volume of sediment evacuated from the debris-flow initiation zone. (C) Total volume of sediment for each period as identified in the airborne LiDAR survey (see Table 1 showing start and end dates of periods 1–6). Sediment volumes in (B) and (C) were estimated from periodic photography of storage. Occurrence of a debris flow sometime between 10 May and 28 June 2013 was identified by field survey, but the exact date of the debris flow could not be specified.

4.2. Airborne LiDAR assessments

Airborne LiDAR data exhibit topographic changes that can be linked to different debris-flow paths of different runout lengths and variations in the areas affected. As can be seen in Fig. 5, all debris-flow material has been deposited within the study zone in 2009, 2010 (period 3), and 2013 (period 6); whereas most debris has been evacuated out of the study reach during the other periods. Flows systematically originated from the uppermost reaches of the study area throughout the time window analyzed, and they were diverted to the south at the confluence with the Hontani torrent. Fig. 6A shows those areas of accumulation for which data has been acquired repetitively over the six periods and for which detection of geomorphic changes is possible. The present-day main path has been a hotspot of activity over the past decade. Deposition occurred mainly in periods 2, 4, and 6 during which the branching of flows on the cone favored significant deposition below channel avulsion points (Fig. 5B, C, E).

Vertical and lateral channel changes were less obvious in the Hontani torrent (Fig. 5). Sediment movements can be recognized on the hillslopes located at the southeastern end of the study area, but these movements were disconnected from the debris-flow system and its fan. We observe, by contrast, that mobilization of sediment from the talus cone, which occurred in the northeastern area of the study area in period 4, did indeed reach the debris-flow fan. However, the largest proportion of this sediment was deposited before it actually reached the debris-flow path of the upper Ichinosawa catchment. Therefore, debris flows originating from the upper Ichinosawa catchment are the main reason for topographic changes at the study site (Fig. 5B, C).

The occurrence of erosion and depositional processes varied considerably in space among survey periods (Fig. 5). For instance, the southern part of the study area was severely eroded by debris flows in period 2 (with erosion depths of >3 m), but remained mostly unaffected during the other periods. Vertical changes >3 m also occurred several times in the main channel, but less frequently in the secondary flow paths. Depositional and erosional features were most obvious in periods 2 and 4, for which we also observe the largest volumes of sediment transfers from the upper Ichinosawa basin. The formation of lobate deposits was also commonly observed over all areas affected by debris flows, except for period 1 for which the formation of lobes could not be confirmed based on slope gradient maps (Fig. 7).

4.3. Orthophoto interpretation

The overall spatial and temporal information derived from orthophotograph interpretation is fairly similar to the results obtained from the airborne LiDAR assessment (Figs. 6, 7), as both sets of pictures were taken by the same flight missions. Nevertheless, a series of differences exist between the data sets for specific parts of the debris-flow path. For example, the debris-flow frequency obtained for the southern

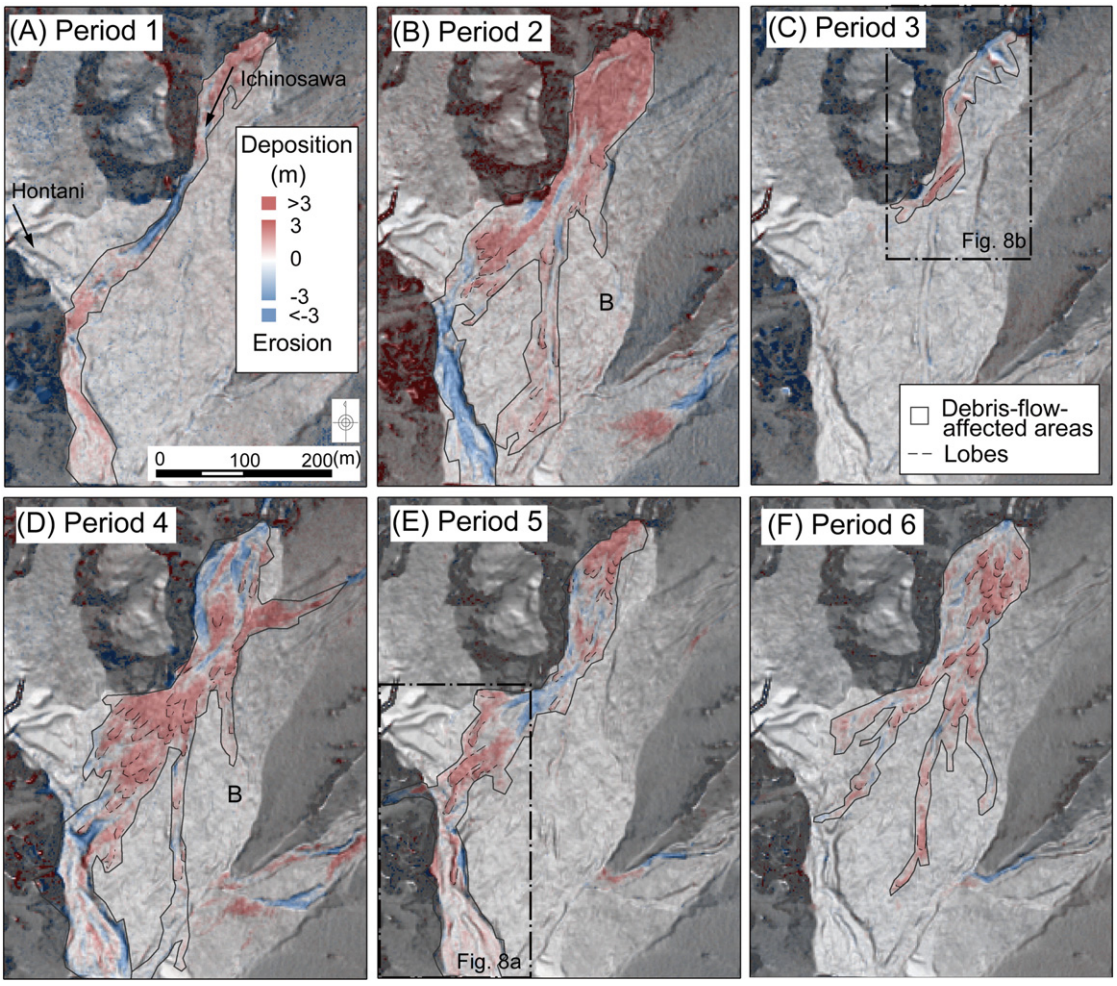

Fig. 5. Changes in ground surface levels in the study area based on periodic airborne LiDAR assessments shaded by the slope gradient calculated from DEMs: (A) period 1 (the 2006 debris-flow season), (B) period 2 (2007 and 2008 debris-flow seasons), (C) period 3 (2009 and 2010 debris-flow seasons), (D) period 4 (2011 debris-flow season), (E) period 5 (2012 debris-flow season), and (F) period 6 (2013 debris-flow season). The outline surrounding erosion and deposition areas describe areas affected by debris flows. Areas around B in (B) and (D) represent a debris-flow path detected by orthophoto interpretation but remaining undetected by airborne LiDAR assessments.

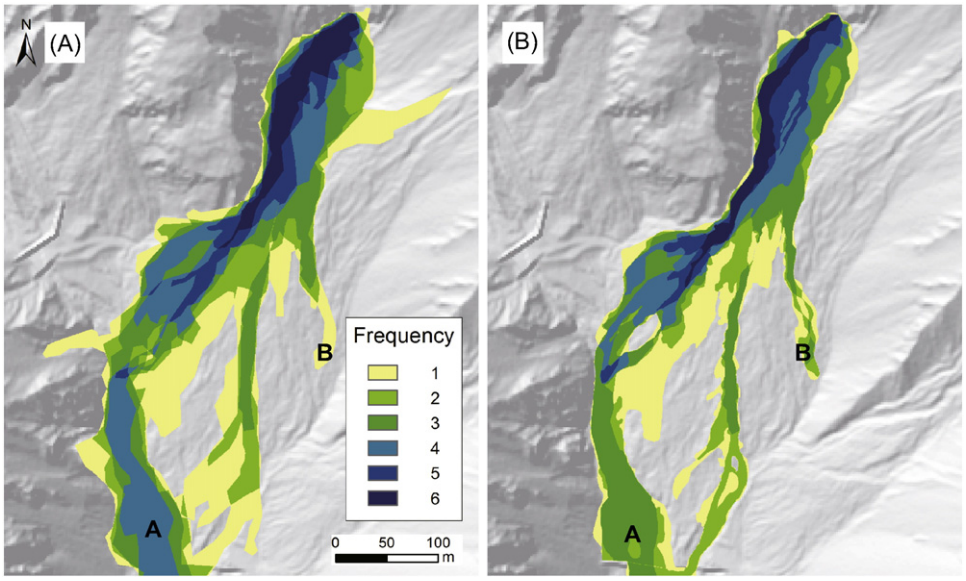

Fig. 6. Frequency of active flow paths over six periods obtained from analysis of (A) LiDAR data and (B) orthophotos. 'A' is a characteristic area for which debris-flow frequency as assessed on orthophotos was lower than that in airborne LiDAR DEMs. 'B', by contrast, is a characteristic area with an opposite relationship.

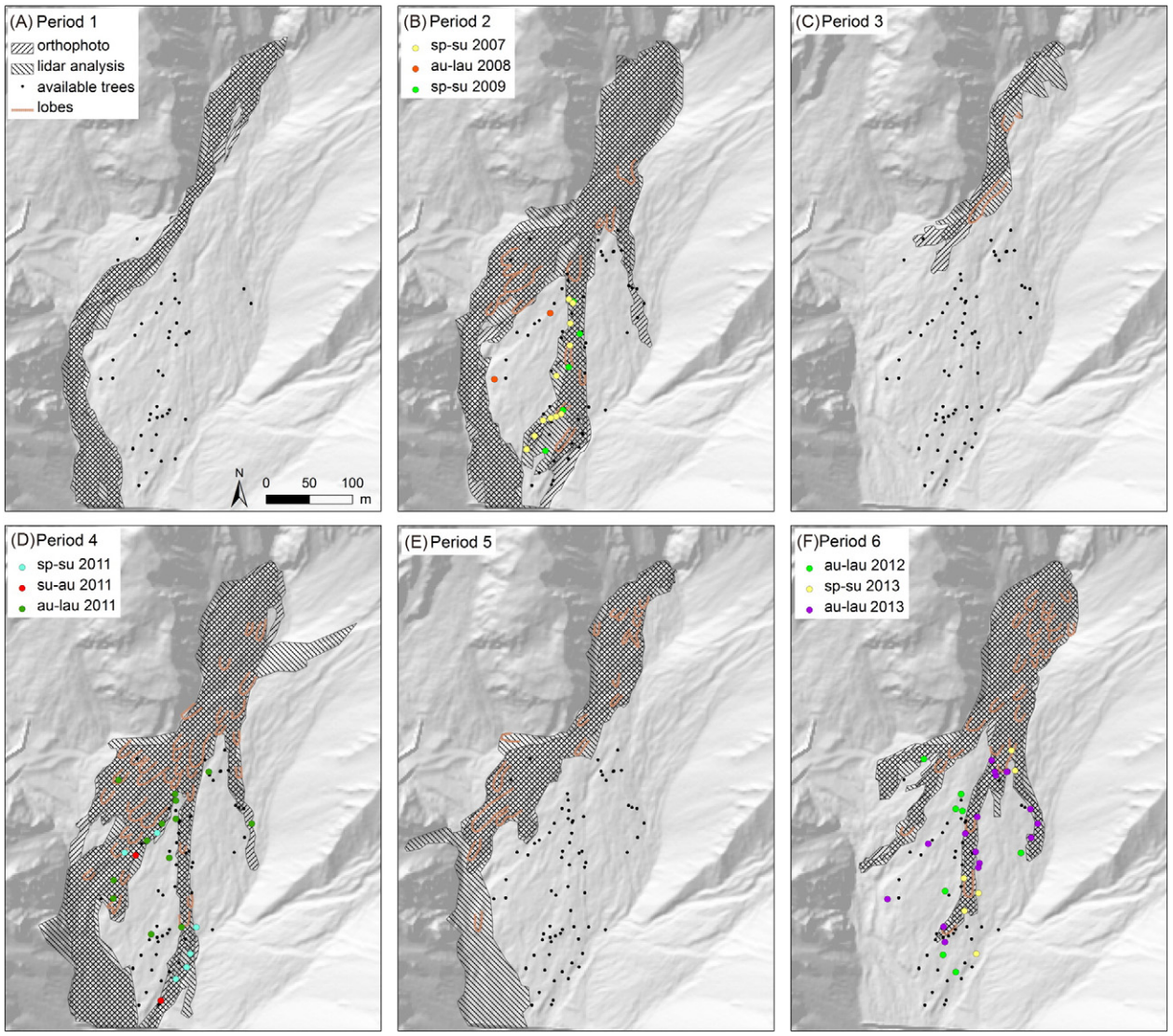

Fig. 7. Debris-flow paths for different periods as estimated by different remotely sensed methods and overlain by dendrogeomorphic data.

part of the main channel (A in Fig. 6) using orthophotographs is lower than that retrieved from airborne LiDAR data. By contrast, we realize that the debris-flow frequency one would reconstruct from orthophtographs in the eastern branch (B in Fig. 6) will be higher than that obtained from airborne LiDAR. When comparing the total area affected by debris flows from the two sets of information, we realize that the debris-flow perimeter in the LiDAR-based record (17.6 ha) is larger by a factor of 1.3 than that obtained from orthophotos (13.9 ha; Table 4). If analyzed for specific periods, differences between the LiDAR-based data orthophotos are reasonably small with 12–16% in periods 1, 2, 4, and 6 but show substantial differences of 41–45% in periods 3 and 5.

4.4. Dendrogeomorphic debris-flow reconstruction

Damage in trees was used to date past debris flows and to infer the intra-annual timing of events, it further served the assessment of spread and reach of individual events. As a result of the complex terrain and frequent activity with multiple reactions and frequent removal of vegetation, however, we only accepted reactions in trees if the latter were arranged in a meaningful way on the cone and if trees showed simultaneous growth disturbances. We also carefully compared the spatial distribution of reacting trees with mapped geomorphic changes and decided to accept an event as soon as at least two trees showed simultaneous reactions.

As debris flows were mostly restricted to the main channel in periods 1 and 5 — with rather limited avulsion activity — we do not observe any injuries in trees during this period and cannot therefore provide any further details on the timing and/or microspatial patterns for these years. We also do not see any damage in trees induced by debris-flow activity in period 3 as events of that time were deposited above the upper forest fringe.

For periods 2, 4, and 6, by contrast, dendrogeomorphology was used successfully to date a series of debris flows, their flow paths, and seasonality of events. By way of example, Fig. 7B yields additional details on a flow affecting the central part of the study area in late spring or early summer 2007 (Fig. 7B). According to the information we have from field surveys and periodical photography, the dating corresponds to the event recorded on 13 June, 2007 (Fig. 4A) and thus allows complementing existing information for the source area with data on the fan. Dendrogeomorphic records also indicate that the debris flow captured by the monitoring system on 5 September 2007 did not clearly damage trees and that the event did not affect the fan (either as a result of early stopping at the fan apex or by remaining constrained to the main channel). We also realize that the dendrogeomorphic record repeatedly suggests that the extent of affected areas obtained from damaged trees is larger than the process areas as derived from other sources. We therefore conclude that dendrogeomorphology can allow inclusion of less severely affected areas that cannot be seen in remotely sensed data as the change in topography will be smaller than the level of uncertainty in the latter techniques.

5. Discussion

In the study presented here, we employed a broad variety of currently available techniques to retrospectively document and describe several dozen debris-flow events that occurred over the past decade in one of the most active debris-flow systems of the Japanese Alps. This study therefore did not only allow assessment of debris-flow process dynamics at the Ohya landslide in detail but also clearly shows that significant differences exist in the quantity and quality of results depending on the approach used. In addition, this contribution also calls for a coupled utilization of different approaches if specific process-related questions have to be answered a posteriori.

Table 4
Affected area obtained using LiDAR DEM and orthophoto interpretation.

Period	LiDAR DEM analysis (ha)	Orthophoto analysis (ha)	Difference (ha)	Difference (%)
1	1.79	1.58	0.21	12
2	4.41	3.68	0.73	16
3	0.75	0.45	0.31	41
4	4.84	4.14	0.70	14
5	3.14	1.71	1.43	45
6	2.70	2.37	0.34	12

By way of example, analysis of LiDAR DEM data and orthophotographs showed quite clearly that the formation of new lobes was limited mostly to the upper part of the fan and to the areas next to the main channel (Fig. 7). Similar trends have been reported in previous work, where topographic features of debris-flow deposits were usually less clearly developed at the lower as compared to the upper part of debris-flow fans (Suwa and Okuda, 1983; Whipple and Dunne, 1992). Because the pattern of lobe formation is affected by sediment concentration (Whipple and Dunne, 1992), lobes tend to develop in the steeper part of the debris-flow fan, which is typically associated with the area of deposition of debris flows with high sediment concentration (Takahashi, 1977, 2014). At the Ohya landslide, the gradient of the main channel drops from ca. 20 to 9° between the upper and lowers parts of the fan, such that hyperconcentrated flows (i.e., flows without coarse particles in the upper flow layer typical for gradients of ca. 10°; Coussot and Meunier, 1996; Takahashi, 2009) would occur in the lower part of the fan. Such low-concentration flows, often mixed with fluvial processes, have presumably contributed to the formation of depositional features lacking clear lobate structures. In addition, and as the area is located downstream of the channel junction with Hontani basin, water supply from the latter may have decreased sediment concentration in the flow and thus may have formed gentler and flatter channel morphologies.

As with many other debris-flow torrents in the world (Whipple and Dunne, 1992; Imaizumi and Sidle, 2007), travel distance of Ohya debris flows varied substantially among events. We observe some relationships between the spatial distribution of debris-flow affected areas (in terms of spread and reach) and the total volume of sediment transported from the initiation zone. During period 3, when annual total volume of sediment transported by debris flows was very small (i.e., 3600 and 4000 m^3 in 2009 and 2010, respectively; Fig. 4), all flows were stopped in the upper part of the study area. By contrast, LiDAR DEM data showed that debris flows were transported beyond the study area in 2007, 2011, and 2012 when total sediment volume exceeded 25,000 m^3. Comparison of the number of debris flows (2 and 5 in 2007 and 2011, respectively) and the total volume of transported sediment (29,000 and 58,000 m^3 in 2007 and 2011, respectively) shows that the total volume of at least one of the debris flows must have exceeded 10,000 m^3. Although debris-flow runout distance is not solely determined by total discharge but also affected by other factors such as solid concentration, channel gradient, catchment area, and rainfall patterns (Whipple and Dunne, 1992; Dadson et al., 2004; Rickenmann, 2005; Imaizumi and Sidle, 2007), our results imply that debris flows with larger total volumes would also have longer travel distances.

In addition, we also demonstrate that the debris-flow path diverged during periods 2 and 5 when debris flows >10,000 m^3 occurred at the study site. We speculate that debris flows with large total volumes tend to diverge at downstream points of the site. Total debris-flow discharge has some relationship with peak discharge (e.g., Ikeda and Hara, 2002) such that discharge of some debris flows in these periods possibly exceeded the conveyance capacity of the main channel, thereby resulting in overbank flow and branching. Sediment deposition is another factor contributing to the branching of debris-flow paths (Whipple and Dunne, 1992); as significant channel-bed aggradation (with depth >2 m) was found around the branching points in periods 2, 4, and 6, it cannot be excluded that these changes may possibly have affected divergence of flows at the Ohya landslide.

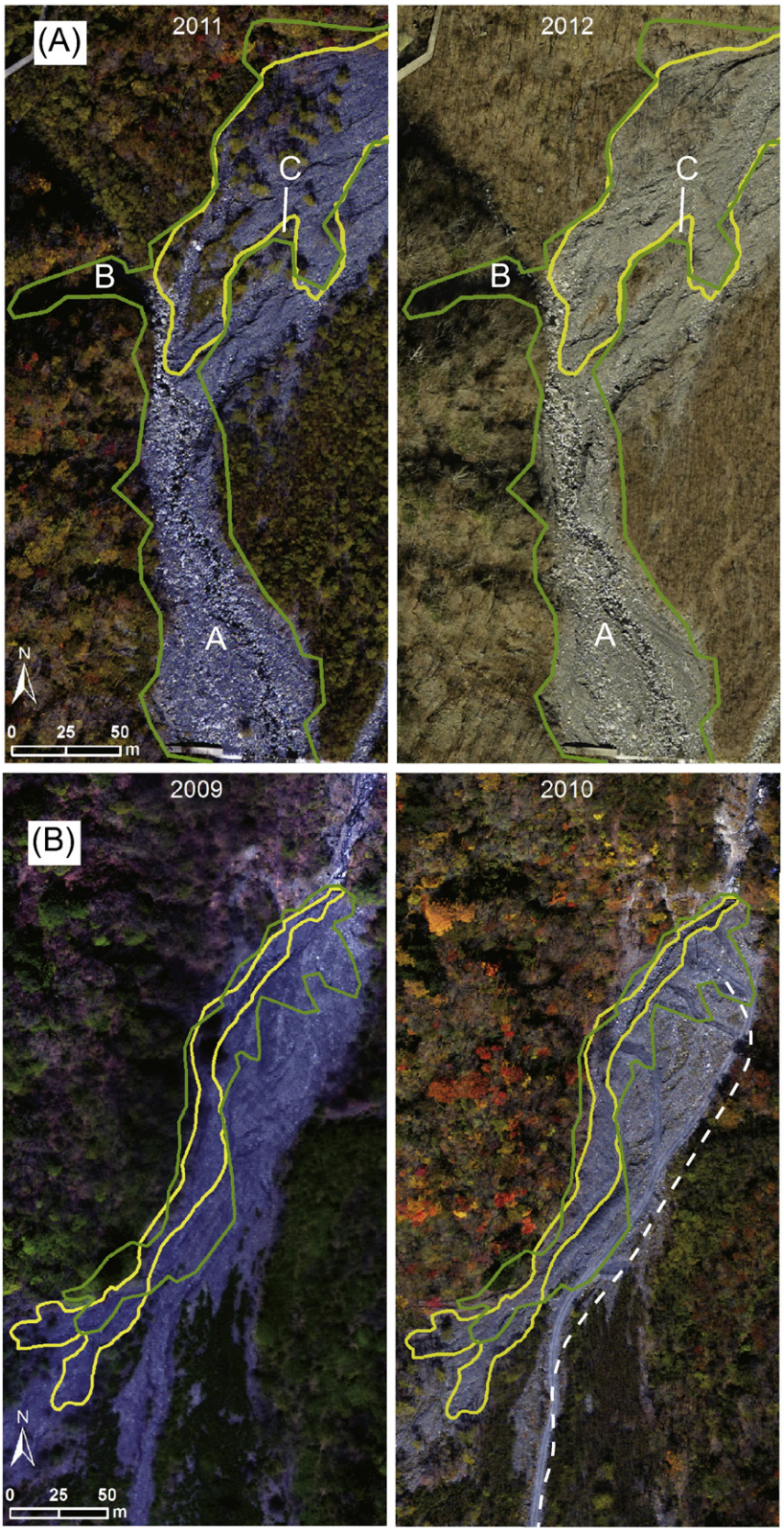

Fig. 8. Area with mismatch between LiDAR (green) and orthophoto (yellow) interpretations of active flow paths in the lower part of the study site. (A) For period 5, sources for errors are areas with shallow modifications (area A) and/or shaded areas (area B) in the orthophotos. Orthophoto interpretation cannot detect changes in topography under tree crowns (area C). (B) For period 3, sources for errors are anthropogenic modifications that could be misinterpreted as debris-flow-related landforms if analysis was solely based on LiDAR data. The dashed line in Fig. 8B indicates a temporary road. Locations of areas shown in Fig. 8 are also illustrated in Fig. 5.

When it comes to the comparison of approaches, we realize that debris-flow affected areas as interpreted from LiDAR data differ significantly from those identified on classical orthophotos (Figs. 2, 6; Table 2). As the differences in area between methods largely exceed the spatial errors inherent to the approaches (Fig. 7), they must be attributed to other sources of errors in area estimation.

The LiDAR assessment generally yielded larger debris-flow surfaces than orthophoto interpretation (Table 4). Several factors may have contributed to these differences: Firstly, orthophoto interpretation has obviously failed to detect those debris-flow areas where topographic changes remained fairly small. For instance, deposition areas with aggradation <0.3 m were widely distributed in the southern part of the study area in period 5 (Fig. 5E). Because this area was lacking vegetation (area A in Fig. 8A), changes in vegetation, such as fallen trees, could not be used as an indicator of debris-flow activity. In addition, we realize that several large boulders have not been moved by debris flows as a result of selective transport of finer sediments, thereby preventing correct recognition of affected area and resulting in substantial differences between the methods (Table 4). In addition, errors from shade and tree crowns also led to an underestimation of areas in the orthophoto interpretation approach (areas B and C in Fig. 8A).

Clear changes in topography can be observed at the lower part of the eastern debris-flow branch in periods 2 and 4 (B in Fig. 5B and D) but were limited to comparably small areas. As a consequence, the LiDAR DEM interpreted these changes as noise and failed to recognize the area as a debris-flow path. By contrast, the area has been detected successfully on the orthophotos (area B in Fig. 6). Consequently, errors in LiDAR DEM interpretation do not necessarily arise from the accuracy of the approach itself (several centimeters in general, and a few dozen centimeters in steep topography; Bremer and Sass, 2012; Imaizumi et al., 2015) but rather from the difficulty in distinguishing elevational changes induced by debris flows from other patterns (i.e., noise). LiDAR assessments also misclassified roads as debris-flow-related landforms (Fig. 8B), resulting in sometimes large differences in mapped areas in period 4 (Table 4). As such, and although LiDAR data are effective in analyzing detailed geomorphic processes in various areas, an interpretation based exclusively on LiDAR analyses may sometimes lead to misinterpretation of real geomorphic processes (Roering et al., 2013).

Areas in which trees are injured but survive cannot easily be used for orthophoto interpretation. By contrast, such areas can be screened for injured trees, and damage can be analyzed and dated using tree-ring approaches (Fig. 7B, D, F). Therefore, mapped debris-flow paths and areas affected by events will be inherently smaller on orthophoto assessments than that derived by tree-ring records. In this sense, tree rings have a certain number of advantages over orthophoto assessments. Activity during period 6 in the central area of the study site is such an example, as events could only be detected by dendrogeomorphology and with a temporal resolution that is much higher than that provided by remotely sensed data (Table 5).

Nevertheless, limitations also exist in dendrogeomorphology: first of all, debris flows can only be analyzed in vegetated areas and events need to be of sufficient size to injure trees while small enough not to kill them. At the Ohya landslide, topography in the main channel is frequently modified by debris flow, such that vegetation recovery is often prevented. Therefore, dendrogeomorphology clearly missed a major proportion of the activity along the main channel. In periods 2 and 6, trees that were located at some distance from the main debris-flow path as mapped in the orthophoto and LiDAR analyses had injuries (Fig. 7B, F). We explain these differences by the nature of the shallow overtopping surges, which cannot be detected with remote sensing techniques, but are still flowing some distance into the forest yet transporting enough debris or woody material to cause tree damage. In period 4, injured trees are located in direct proximity to debris-flow lobes so that several events of this period could be dated with subseasonal resolution. If landforms of past debris-flow activity are conserved, tree-ring series can indeed contribute substantially to frequency-magnitude relations of debris flows (Stoffel et al., 2008; Stoffel, 2010), sometimes even over several centuries. Such extraordinarily long reconstructions can be realized in case high-resolution geomorphic mapping of landforms related to debris-flow activity exists and that trees affected by debris flows are not killed by events. The system at the Ohya landslide is somewhat different from many debris-flow environments in the Alps in the sense that it is only partly vegetated by primarily young broadleaves that are frequently removed by debris flows (Bollschweiler and Stoffel, 2010; Procter et al., 2011, 2012; Schneuwly-Bollschweiler and Stoffel, 2012). Another possible reason for these differences in process-vegetation interactions may be related to topographic conditions and the setting of the Ohya landslide fan in a steep and narrow river valley, which indeed limits lateral spread of flows and thus decreases the probability for well-preserved lobes. As a result, we also realize that the remaining landforms at the Ohya landslide are interwoven in a complex manner and frequently modified by subsequent generations of debris flows, which in turn hamper larger tree ages (with tree age also being related to the species growing at the site and thus local climate) and the establishment of long tree-ring chronologies.

In terms of temporal resolution, the present study could rely on a fairly large number of both LiDAR and orthophoto documents, i.e., roughly one set of illustrations every single or at least every second year. The frequency of assessments as available at the Ohya landslide to improve sediment control may not exist at other sites, and such intensive monitoring is limited to a few sites worldwide because of the high costs involved. Therefore, and under other conditions, we conclude that the temporal resolution of tree-ring assessments would generally exceed that of LiDAR and orthophoto assessments and should be preferred where available, at least when it comes to the detection of individual events and the establishment of chronologies of fans with a reasonable tree cover. Even at the Ohya landslide, the intervals of airborne LiDAR and aerial photograph surveys are still longer than the

Table 5
Summary of methods for interpretation of debris flow.

Name of methods	Key details	Advantages	Limitations	Roles in multimethod monitoring
Field monitoring	Observation of flow dynamics, geomorphic changes	High temporal resolution (diurnal)	Time and effort needed for the monitoring	Detection of timing of debris flows
LiDAR DEM analysis	Geomorphic changes	High spatial resolution	Difficulty in distinguishing between local topographic changes and noise, low temporal resolution, costs	Interpretation of debris-flow-affected areas
Orthophoto interpretation	Changes in the vegetation, movement of large boulders, geomorphic changes	Discrimination of debris flow path and other patterns (noise, artificial change)	Missing of small geomorphic changes, errors caused by the tree crown and shade, low temporal resolution	Removal of errors in LiDAR DEM analysis
Dendrogeomorphology	Injuries in tree ring	High temporal resolution (subseasonal), reconstruction of longer debris-flow histories	Not available in nonvegetated areas, killing of trees by large debris flow events.	Improvement of temporal resolution, Detection of small events without clear geomorphic change

intervals of debris flows in the catchment. Thus, remotely-sensed approaches cannot necessarily recognize the area affected by an individual debris-flow event. Our dendrogeomorphic approach successfully dated debris-flow-affected areas with seasonal accuracy in 3 out of 6 periods (Fig. 7), a resolution that was hardly achieved by LiDAR and orthophoto assessments. Therefore, field-based dendrogeomorphology remains most useful when it comes to the discussion and documentation of debris flows at annual or seasonal timescales. On the other hand, dendrogeomorphology cannot solely draw the outline of debris-flow-affected areas in this study area because of the limited number of the sampled trees and the absence of trees in a large part of the debris-flow fan. Reconstruction of debris-flow histories at the Ohya landslide with high spatial and temporal resolution can be achieved by applying dendrogeomorphology, which has high temporal resolution, to the debris-flow-affected areas detected by airborne LiDAR and orthophotograph interpretations, which have high spatial resolution.

6. Conclusions

In this study we investigated the debris-flow history at the Ohya landslide (central Japan) by using multiple methods including field monitoring, airborne LiDAR DEM analysis, orthophoto interpretation, and tree-ring assessments. Comparison of debris-flow-affected areas assessed by these methods showed agreement on the larger patterns in general but also unveiled considerable mismatches among the methods. Each approach has a certain number of advantages and limitations. We realize that orthophoto interpretation usually underestimates areas affected by debris flows as it ignores small changes in topography. In addition, debris-flow paths in shady and/or tree-crowned areas cannot be identified in the photographs either, and are thus also affecting underestimation of orthophoto assessments. Airborne LiDAR assessments have some advantage in the interpretation of debris flows in the area with incised topography or vegetation cover. On the other hand, limitations in airborne LiDAR interpretation are related to their difficulty in distinguishing between local topographic changes and noise.

A combination of multiple methods may overcome the weaknesses of each single method. For example, the combination of airborne LiDAR and orthophoto interpretation can improve the spatial resolution and delineation of areas affected by debris flows. In addition, dendrogeomorphology may help to improve temporal resolution in case that the area under investigation supports trees. Accordingly, the combination of these methods permits assessment of the debris-flow history with high spatial and temporal resolution.

Acknowledgement

This work was supported by JSPS KAKENHI Grant Numbers 26282076 and 26292077, Research and Education Funding for the Japanese Alps Inter-Universities Cooperative Project, MEXT Japan, and a research grant from University of Tsukuba. The Shizuoka River Office, Ministry of Land, Infrastructure, Transport and Tourism, Japan, kindly provided airborne LiDAR data and orthophotographs.

References

Alestalo, J., 1971. Dendrochronological interpretation of geomorphic processes. Fennia 105, 1–139.

Allen, S.K., Rastner, P., Arora, M., Huggel, C., Stoffel, M., 2015. Lake outburst and debris flow disaster at Kedarnath, June 2013: hydrometeorological triggering, and topographic predisposition. Landslides http://dx.doi.org/10.1007/s10346-015-0584-3 (in press).

Arattano, M., Marchi, L., Cavalli, M., 2012. Analysis of debris-flow recordings in an instrumented basin: confirmations and new findings. Nat. Hazards Earth Syst. Sci. 12, 679–686.

Arbellay, E., Stoffel, M., Bollschweiler, M., 2010. Wood anatomical analysis of *Alnus incana* and *Betula pendula* injured by a debris-flow event. Tree Physiol. 30, 1290–1298. http://dx.doi.org/10.1093/treephys/tpq065.

Arbellay, E., Stoffel, M., Sutherland, E.K., Smith, K.T., Falk, D.A., 2014a. Changes in tracheid and ray traits in fire scars of North American conifers and their ecophysiological implications. Ann. Bot. 114, 223–232.

Arbellay, E., Stoffel, M., Sutherland, E.K., Smith, K.T., Falk, D.A., 2014b. Resin duct size and density as ecophysiological traits in fire scars of *Pseudotsuga menziesii* and *Larix occidentalis*. Ann. Bot. 114, 973–980.

Berger, C., McArdell, B.W., Schlunegger, F., 2011a. Direct measurement of channel erosion by debris flows, Illgraben, Switzerland. J. Geophys. Res. 116, F01002. http://dx.doi.org/10.1029/2010JF001722.

Berger, C., McArdell, B.W., Schlunegger, F., 2011b. Sediment transfer patterns at the Illgraben catchment, Switzerland. Implications for the time scales of debris flow activities. Geomorphology 125, 421–432.

Bollschweiler, M., Stoffel, M., 2010. Tree rings and debris flows: recent developments, future directions. Prog. Phys. Geogr. 34, 625–645. http://dx.doi.org/10.1177/0309133310370283.

Bollschweiler, M., Stoffel, M., Ehmisch, M., Monbaron, M., 2007. Reconstructing spatio-temporal patterns of debris-flow activity using dendrogeomorphological methods. Geomorphology 87, 337–351. http://dx.doi.org/10.1016/j.geomorph.2006.10.002.

Brardinoni, F., Hassan, M.A., Rollerson, T., Maynard, D., 2009. Colluvial sediment dynamics in mountain drainage basins. Earth Planet. Sci. Lett. 284, 310–319.

Brardinoni, F., Slaymaker, O., Hassan, M.A., 2003. Landslide inventory in a rugged forested watershed: a comparison between air-photo and field survey data. Geomorphology 54, 179–195.

Bremer, M., Sass, O., 2012. Combining airborne and terrestrial laser scanning for quantifying erosion and deposition by a debris flow event. Geomorphology 138, 49–60.

Cornamusini, G., Elter, F.M., Sandrelli, F., 2002. The Corsica–Sardinia massif as source area for the early northern Apennines foredeep system: evidence from debris flows in the "Macigno costiero" (late Oligocene, Italy). Int. J. Earth Sci. 91, 280–290.

Coussot, P., Meunier, M., 1996. Recognition, classification and mechanical description of debris flows. Earth Sci. Rev. 3–4, 209–227.

Crosta, G.B., Frattini, P., 2004. Controls on modern alluvial fan processes in the central Alps, northern Italy. Earth Surf. Process. Landf. 29, 267–293.

Cui, P., Hu, K., Zhuang, J., Yang, Y., Zhang, J., 2011. Prediction of debris-flow danger area by combining hydrological and inundation simulation methods. J. Mt. Sci. 8, 1–9. http://dx.doi.org/10.1007/s11629-011-2040-8.

Dadson, S.J., Hovius, N., Chen, H., Dade, B., Lin, J.C., Hsu, M.L., Lin, C.W., Horng, M.J., Chen, T.C., Milliman, J., Stark, C.P., 2004. Earthquake-triggered increase in sediment delivery from an active mountain belt. Geology 32, 733–736.

Fannin, R.J., Wise, M.P., 2001. An empirical-statistical model for debris flow travel distance. Can. Geotech. J. 38 (5), 982–994. http://dx.doi.org/10.1139/t01-030.

Frankel, K.L., Dolan, J.F., 2007. Characterizing arid region alluvial fan surface roughness with airborne laser swath mapping digital topographic data. J. Geophys. Res. 112, F02025. http://dx.doi.org/10.1029/2006JF000644.

Glade, T., 2005. Linking debris-flow hazard assessment with geomorphology. Geomorphology 66, 189–213.

de Haas, T., Ventra, D., Carbonneau, P., Kleinhans, M., 2014. Debris-flow dominance of alluvial fans masked by runoff reworking and weathering. Geomorphology 217, 165–181. http://dx.doi.org/10.1016/j.geomorph.2014.04.028.

Hu, K., Wei, F., Li, Y., 2011. Real-time measurement and preliminary analysis of debris-flow impact force at Jiangjia Ravine, China. Earth Surf. Process. Landf. 36, 1268–1278.

Hughes, M.L., McDowell, O.F., Marcus, W.A., 2006. Accuracy assessment of georectified aerial photographs: implications for measuring lateral channel movement in a GIS. Geomorphology 74, 1–16. http://dx.doi.org/10.1016/j.geomorph.2005.07.001.

Hupp, C.R., 1984. Dendrogeomorphic evidence of debris flow frequency and magnitude at Mount Shasta, California. Environ. Geol. Water Sci. 6, 121–128.

Hürlimann, M., Rickenmann, D., Graf, C., 2003. Field and monitoring data of debris-flow events in the Swiss Alps. Can. Geotech. J. 40, 161–175.

Ikeda, A., Hara, Y., 2002. Debris flows generated at Kitamata Valley of the Name River. Proceedings of INTERPRAEVENT 2002 in the Pacific Rim 1, pp. 101–112.

Imaizumi, F., Sidle, R.C., 2007. Linkage of sediment supply and transport processes in Miyagawa Dam catchment, Japan. J. Geophys. Res. 112, F03012. http://dx.doi.org/10.1029/2006JF000495.

Imaizumi, F., Nishi, R., Murakami, W., Daimaru, H., 2015. Parallel retreat of rock slopes underlain by alternation of strata. Geomorphology 238, 27–36. http://dx.doi.org/10.1016/j.geomorph.2015.02.030.

Imaizumi, F., Sidle, R.C., Kamei, R., 2008. Effects of forest harvesting on the occurrence of landslides and debris flows in steep terrain of central Japan. Earth Surf. Process. Landf. 33, 827–840.

Imaizumi, F., Sidle, R.C., Tsuchiya, S., Ohsaka, O., 2006. Hydrogeomorphic processes in a steep debris flow initiation zone. Geophys. Res. Lett. 33, L10404. http://dx.doi.org/10.1029/2006GL026250.

Imaizumi, F., Tsuchiya, S., Ohsaka, O., 2005. Behaviour of debris flows located in a mountainous torrent on the Ohya landslide. Japan. Can. Geotech. J. 42, 919–931.

Iverson, M.R., 1997. The physics of debris flows. Rev. Geophys. 35, 245–296. http://dx.doi.org/10.1029/97RG00426.

Jakob, M., Bovis, M., Oden, M., 2005. The significance of channel recharge rates for estimating debris-flow magnitude and frequency. Earth Surf. Process. Landf. 30, 755–766.

Keefer, D.K., Moseley, E.M., deFrance, S.D., 2003. A 38 000-year record of foods and debris fows in the Ilo region of southern Peru and its relation to El Niño events and great earthquakes. Palaeogeogr. Palaeoclimatol. Palaeoecol. 194, 41–77.

Lin, P.S., Lin, J.Y., Hung, J.C., Yang, M.D., 2002. Assessing debris-flow hazard in a watershed in Taiwan. Eng. Geol. 66, 295–313. http://dx.doi.org/10.1016/S0013-7952(02)00105-9.

Mackey, B.H., Roering, J.J., 2011. Sediment yield, spatial characteristics, and the long term evolution of active earthflows determined from airborne LiDAR and historical aerial photographs, Eel River, California. Geol. Soc. Am. Bull. 123 (7–8), 1560–1576.

March, L., Arattano, M., Deganutti, A.M., 2002. Ten years of debris-flow monitoring in the Morcardo Torrent (Italian Alps). Geomorphology 46, 1–17. http://dx.doi.org/10.1016/S0169-555X(01)00162-3.

Procter, E., Bollschweiler, M., Stoffel, M., Neumann, M., 2011. A regional reconstruction of debris-flow activity in the Northern Calcareous Alps, Austria. Geomorphology 132, 41–50.

Procter, E., Stoffel, M., Bollschweiler, M., Neumann, M., 2012. Exploring debris-flow history and process dynamics using an integrative approach on a dolomitic cone in western Austria. Earth Surf. Process. Landf. 37, 913–922.

Rickenmann, D., 2005. Runout prediction methods. In: Jakob, M., Hunger, O. (Eds.), Debris Flow Hazards and Related Phenomena, Praxis. Spromger, Berlin Heidelberg, pp. 305–324.

Roering, J.J., Mackey, B.H., Marshall, J.A., Sweeney, K.E., Deligne, N.I., Booth, A.M., Booth, A.M., Handwerger, A.L., Cerovski-Darriau, C., 2013. 'You are HERE': connecting the dots with airborne lidar for geomorphic fieldwork. Geomorphology 200, 172–183.

Schneuwly-Bollschweiler, M., Stoffel, M., 2012. Hydrometeorological triggers of periglacial debris flows — a reconstruction dating back to 1864. J. Geophys. Res. 117, F02033.

Schneuwly-Bollschweiler, M., Corona, C., Stoffel, M., 2013. How to improve dating quality and reduce noise in tree-ring based debris-flow reconstructions. Quat. Geochronol. 18, 110–118. http://dx.doi.org/10.1016/j.quageo.2013.05.001.

Shroder Jr., J.F., 1978. Dendrogeomorphological analysis of mass movement on Table Cliffs Plateau, Utah. Quat. Res. 9, 168–185. http://dx.doi.org/10.1016/0033-5894(78)90065-0.

Staley, D.M., Wasklewicz, T.A., Blaszczynsk, J.S., 2006. Surficial patterns of debris flow deposition on alluvial fans in Death Valley, CA using airborne laser swath mapping data. Geomorphology 74, 152–163. http://dx.doi.org/10.1016/j.geomorph.2005.07.014.

Stoffel, M., 2010. Magnitude-frequency relationships of debris flows — a case study based on field surveys and tree-ring records. Geomorphology 116, 67–76.

Stoffel, M., Bollschweiler, M., 2008. Tree-ring analysis in natural hazards research — an overview. Nat. Hazards Earth Syst. Sci. 8, 187–202. http://dx.doi.org/10.5194/nhess-8-187-2008.

Stoffel, M., Corona, C., 2014. Dendroecological dating of geomorphic disturbance in trees. Tree-Ring Res. 70, 3–20http://dx.doi.org/10.3959/1536-1098-70.1.3.

Stoffel, M., Hitz, O.M., 2008. Snow avalanche and rockfall impacts leave different anatomical signatures in tree rings of *Larix decidua*. Tree Physiol. 28, 1713–1720.

Stoffel, M., Perret, S., 2006. Reconstructing past rockfall activity with tree rings: some methodological considerations. Dendrochronologia 24 (1), 1–15.

Stoffel, M., Bollschweiler, M., Beniston, M., 2011. Rainfall characteristics for periglacial debris flows in the Swiss Alps: past incidences — potential future evolutions. Clim. Chang. 105, 263–280. http://dx.doi.org/10.1007/s10584-011-0036-6.

Stoffel, M., Bollschweiler, M., Butler, D.R., Luckman, B.H., 2010. Tree Rings and Natural Hazards. Springer, Dordrecht, New York.

Stoffel, M., Butler, D.R., Corona, C., 2013. Mass movements and tree rings: a guide to dendrogeomorphic field sampling and dating. Geomorphology 200, 106–120. http://dx.doi.org/10.1016/j.geomorph.2012.12.017.

Stoffel, M., Conus, D., Grichting, M.A., Lièvre, I., Maître, G., 2008. Unraveling the patterns of late Holocene debris-flow activity on a cone in the Swiss Alps: chronology, environment and implications for the future. Glob. Planet. Chang. 60, 222–234. http://dx.doi.org/10.1016/j.gloplacha.2007.03.001.

Stoffel, M., Lièvre, I., Monbaron, M., Perret, S., 2005. Seasonal timing of rockfall activity on a forested slope at Täschgufer (Valais, Swiss Alps) — a dendrochronological approach. Z. Geomorphol. 49 (1), 89–106.

Stoffel, M., Mendlik, T., Schneuwly-Bollschweiler, M., Gobiet, A., 2014a. Possible impacts of climate change on debris-flow activity in the Swiss Alps. Clim. Chang. 122, 141–155.

Stoffel, M., Tiranti, D., Huggel, C., 2014b. Climate change impacts on mass movements — case studies from the European Alps. Sci. Total Environ. 493, 1255–1266.

Suwa, H., Okuda, S., 1983. Deposition of Debris Flows on a Fan Surface, Mt. Yakedake, Japan. Z. Geomorphol. Suppl. 46, 79–101.

Suwa, H., Okano, K., Kanno, T., 2011. Forty years of debris-flow monitoring at Kamikamihorizawa Creek. Mount Yakedake, Japan. In: Genevois, R., Hamilton, D.L., Prestininzi, A. (Eds.), Proceedings of the 5th International Conference on Debris Flow Hazards Mitigation, Mechanics, Prediction and Assessment, pp. 605–613.

Takahashi, T., 1977. An occurrence mechanism of mud-debris flows, and their characteristics in motion. Annuals, DPRI, 23B2, pp. 405–435 (in Japanese).

Takahashi, T., 2009. A review of Japanese debris flow research. Int. J. Erosion Control Eng. 2 (1), 1–14.

Takahashi, T., 2014. Debris Flow: Mechanics, Prediction and Countermeasures. 2nd ed. CRC Press, Boca Raton, Florida (572 pp.).

Trappmann, D., Stoffel, M., 2013. Counting scars on tree stems to assess rockfall hazards: a low effort approach, but how reliable? Geomorphology 180–181, 180–186.

Tsuchiya, S., Imaizumi, F., 2010. Large sediment movement caused by the catastrophic Ohya-kuzure landslide. J. Disaster Sci. 3 (5), 257–263.

Van Steijn, H., 1996. Debris-flow magnitude–frequency relationships for mountainous regions of Central and Northwest Europe. Geomorphology 15, 259–273.

Whipple, K.X., Dunne, T., 1992. The influence of debris-flow rheology on fan morphology, Owens Valley, California. Geol. Soc. Am. Bull. 104, 887–900.

Wieczorek, G., Glade, T., 2005. Climatic factors influencing triggering of debris flows. In: Jakob, M., Hungr, O. (Eds.), Debris Flow Hazards and Related Phenomena. Springer, Heidelberg, pp. 325–362.

Worni, R., Huggel, C., Clague, J.J., Schaub, Y., Stoffel, M., 2014. Coupling glacial lake impact, dam breach, and flood processes: a modeling perspective. Geomorphology 224, 161–176. http://dx.doi.org/10.1016/j.geomorph.2014.06.031.

Zhang, S., 1993. A comprehensive approach to the observation and prevention of debris flows in China. Nat. Hazards 7, 1–23.

Zhang, S., Cheng, J., 2003. Measurement of debris-flow surface characteristics through closerange photogrammety. Proceedings of Debris-flow Hazard Mitigation: Mechanics, Prediction, and Assessment, Davos, Switzerland. Millpress, Rotterdam, pp. 775–784.